JOURNAL OF SPACECRAFT AND ROCKETS
Vol. 34, No. 2, March–April 1997

Aerodynamic Forces and Moments for a Re-Entry Module

J. Allègre,* M. Raffin,† and J. C. Lengrand‡
Centre National de la Recherche Scientifique, Meudon 92190, France
and
A. Chpoun§
Université d'Evry, Evry 91000, France

Experimental investigations have been carried out to characterize the aerodynamic behavior of a re-entry body, based on the Apollo shape, at rarefied and hypersonic flow conditions. The present experiments have been conducted at a Mach number close to 20 and at rarefaction levels covering the near-continuum and transitional flow regimes. Measured aerodynamic forces are compared with calculated Navier–Stokes values using both slip and no-slip boundary treatments and with previous experimental results obtained at the Arnold Engineering Development Center and at the Deutsche Luft and Raumfahrt at Gottingen. For the capsule at 0-deg angle of attack, the drag coefficient is presented as a function of the flow rarefaction from the continuum to the free molecular limit. Force data are also given for angles of attack ranging from 0 to 50 deg, whereas previous experimental data were mostly limited to lower angles of attack of 25 or 35 deg.

Nomenclature

C_A = axial-force coefficient
C_D = drag coefficient
C_N = normal-force coefficient
D = model diameter, mm
Kn = Knudsen number
M = freestream Mach number
p_0 = stagnation pressure, bar
Re = freestream Reynolds number
Re_1 = Reynolds number based on model diameter and upstream flow conditions
Re_2 = Reynolds number based on model diameter and flow conditions behind a normal shock
S = reference area, m^2
T_0 = stagnation temperature, K
V = freestream velocity, m/s
$\bar{V}$ = rarefaction parameter, $M/\sqrt{Re_1}$
X_{cp} = center-of-pressure abscissa, m
α = angle of attack, deg
γ = ratio of specific heats
λ = mean free path, mm

Introduction

THERE is a renewed interest in capsule-type vehicles within the framework of the European Manned Transportation Program (MSTP). An atmospheric re-entry demonstrator (ARD),[1] launched by Ariane 5, will provide more information about some critical re-entry features. The ARD vehicle, based on the Apollo shape and equipped with control jets to ensure high maneuverability, has been selected to satisfy a ballistic re-entry representative of the future European crew transport vehicle (CTV). To predict re-entry flight characteristics, efforts have been undertaken to reactivate research activities on capsules, using experimental as well as numerical approaches.

Received March 10, 1996; revision received Aug. 3, 1996; accepted for publication Oct. 5, 1996.

*Research Scientist, Hypersonic and Rarefied Flow Division.
†Research Engineer, Hypersonic and Rarefied Flow Division.
‡Leading Scientist, Hypersonic and Rarefied Flow Division. Member AIAA.
§Assistant Professor, Mechanical Department, Institute Universitaire de Technologie.

During the 1960s, measurements of aerodynamic coefficients were taken[2,3] on the Apollo Command Module. Comparisons between the results of these measurements and real-flight data showed discrepancies, which were partly explained by real-gas effects and the asymmetrical character of the ablated heat shield on the vehicle during the re-entry phase. Later, complementary experiments were performed on the Apollo Module in the range of transitional and near-free-molecule flows.[4]

Recently, the need for defining aerodynamic characteristics of highly maneuverable capsules and over a wider range of flow conditions required additional wind-tunnel investigations. The present study intends to provide complementary aerodynamic data to characterize the capsule dynamic stability in the range of transitional flow regimes and at angles of attack as large as 50 deg. Experiments were performed in the SR3 wind tunnel of the Centre National de la Recherche Scientifique (CNRS) at Meudon. Measurements of aerodynamic forces and moments were taken for flow conditions characterized by a Mach number close to 20 and a rarefaction parameter ranging approximately from 0.1 to 0.8. In addition to experimental data, aerodynamic forces were also calculated using a Navier–Stokes (NS) solver. At high altitudes, rarefaction effects occur and a kinetic description of the flow has to be substituted for the continuum approach; however, this molecular description requires large computational ressources. In the transitional and near-continuum regimes, continuum methods together with special treatments of wall boundary conditions (e.g., velocity and temperature jump conditions at the wall) offer a computationally more efficient alternative to the molecular approach [e.g., direct simulation Monte Carlo (DSMC) methods].

Another aim of the present work is to verify the validity of such a continuum approach by comparing with experimental data when the incoming flow rarefaction varies. Previous studies, including both kinetic and continuum approaches, were focused on the comparison between experimental and calculated surface quantities and flowfields over a plate, a compression ramp,[5] and around a blunt cone,[6] whereas the present calculations focus on the aerodynamic forces of capsule configurations.

Experimental Flow Conditions and Test Program

The SR3 wind tunnel generates rarefied hypersonic nitrogen flows in a continuous working operation. The test chamber can be connected with two different pumping groups. The first group includes oil-diffusion booster pumps and volumetric vacuum pumps that provide volume flow rates of about 40 m^3/s under pumping pressures of less than a few pascals. The second pumping group, composed

Table 1 Flow conditions

Test cond.	M	p_0, bars	T_0, K	Re/cm	D, mm	Re_1	Re_2	$\bar{V}$	λ, mm	Kn
A	20.2	3.5	1,100	284	25	710	15.8	0.758	0.672	0.0269
B	20.2	3.5	1,100	284	45	1,278	28.4	0.565	0.672	0.0149
C	20.2	10	1,100	811	45	3,650	81.3	0.334	0.235	0.0052
D	20.9	120	1,300	6,851	45	30,830	688	0.119	0.028	0.0006

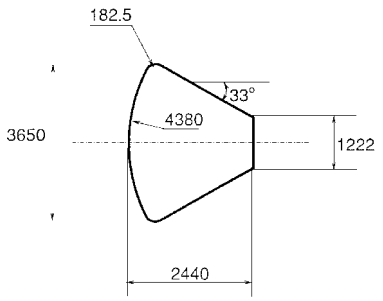

Fig. 1 Full-scale re-entry module; dimensions in millimeters.

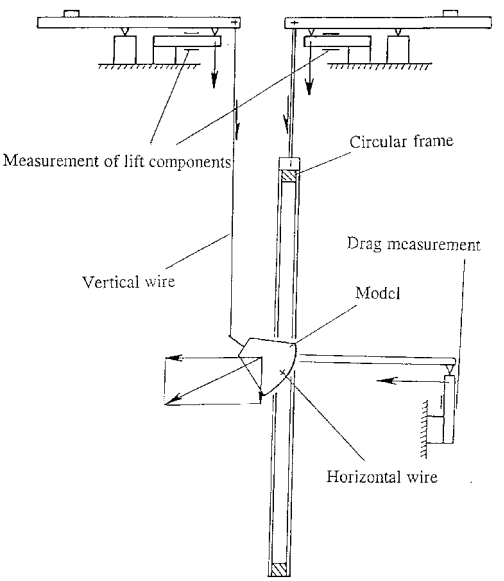

Fig. 2 Balance and model setup.

of volumetric vacuum pumps and large rotary sliding vane pumps, allows larger mass flow rates under higher pumping pressures. This last configuration is used to generate hypersonic-flow conditions at intermediate Reynolds numbers up to 10^5.

Nozzle-flow calibrations illustrate the existence of Mach gradients through the test section. Depending on the test conditions, Mach gradients dM/M are limited to 3–5% over a distance of 10 cm measured in the test section along the nozzle centerline. Transversely, ahead of the front section of the largest test model (45 mm of base diameter), radial Mach gradients correspond to dM/M values of about 4, 2, and 1%, respectively, for the test conditions with stagnation pressures of 3.5, 10, and 120 bars. Reference Mach numbers in the freestream correspond to the model nose coordinates. Because of the low stagnation temperatures of the wind tunnel (1100 or 1300 K according to the test conditions), no real-gas effects and no thermochemical nonequilibrium effects are expected for the present study. On the other hand, wall-slip effects are significant for the rarefied flow regimes presently investigated.

The test program includes four test conditions corresponding to various rarefaction levels. Table 1 summarizes the wind-tunnel conditions, Mach number, stagnation pressure and temperature, the diameter of the models, the values of the Reynolds number upstream and downstream of a normal shock, a rarefaction parameter defined as $M/\sqrt{Re}$, the mean free path as defined by Bird,[7] and the Knudsen number. Reynolds numbers have been calculated using the Sutherland viscosity law for gas temperatures down to 100 K; a linear viscosity law is then used at lower gas temperatures between 0 and 100 K. For each one of the four test conditions, six angles of attack of the model (i.e., 0, 10, 20, 30, 40, and 50 deg) have been considered.

Models

The dimensions of the full-scale module are shown in Fig. 1. The two models used for force measurements in the wind tunnel are made out of aluminum with the diameters $D = 25$ and 45 mm. For the calculation of the aerodynamic coefficients, the reference area is the area of the main cross section ($S = \pi D^2/4$) and the reference length is the model diameter. The origin chosen for presenting the center of pressure is the nose of the model.

Because of the model protection prior to the measurement and also because of the short time period (a few seconds) required for force measurements, the wall temperature of the model did not increase more than 50 K during the run. The wall temperature was close to 350 K at the time of the measurement.

Aerodynamic Balance

External balances have been designed for the SR3 test section. For the present tests, the balance used is schematically presented in Fig. 2. It allows the determination of drag, lift, pitching moment, and center of pressure. The model is connected to the balance by means of two wires, which are 0.2 mm in diameter. One horizontal wire passes through the model in the front part region, and another vertical wire leads to a thin sting screwed on the base of the model.

Basically, the balance consists of three separate dynamometers. The lift acts on two dynamometers while the drag acts on the third one. A circular frame surrounding the test section provides the tension of the horizontal wire. This frame transmits both the drag and the front component of the lift to the corresponding dynamometers. The rear component of the lift is transmitted by means of the vertical wire. In force measurements, the drag of the horizontal wire is subtracted from the total model drag. The drag of the vertical wire is avoided by simply covering and insulating the wire from the flow effects. Based on the balance characteristics and on the data-acquisition process, the maximum uncertainty in force measurement is less than 4% in the most unfavorable case, which corresponds to the most rarefied flow conditions.

Starting the Wind Tunnel and Force Measurements

At the present test conditions, the investigated shape of blunt models makes flow establishment difficult. Consequently, a specific mechanical device has been set up to improve the flow starting conditions when the model remains located within the test section and also to provide the model protection from the shock waves generated when starting and stopping the nozzle flow. The mechanical device is mainly composed of a movable cone (with a 4-cm-base diameter and 25-deg half-cone angle) mounted at the end of a streamlined support, which provides the connection with a pneumatic jack. The cone can be introduced or removed from the test section within a fraction of a second.

Before starting or shutting down the nozzle flow, the cone is injected through the test section, just upstream of the model. The cone apex is then located 6 cm ahead of the model nose. The cone, with its slender shape, facilitates the nozzle flow starting with production of an attached shock at the tip of the cone. At the same time, the cone represents a shield for the model and, thus, limits the convective heating and temperature increase at the model wall. The following procedure is used to measure aerodynamic forces: 1) the model is installed on the balance within the test section at the required angle of attack, 2) the protecting cone is moved in through the test section just ahead of the model, 3) the nozzle flow is started and the stagnation pressure and temperature are stabilized to their correct value,

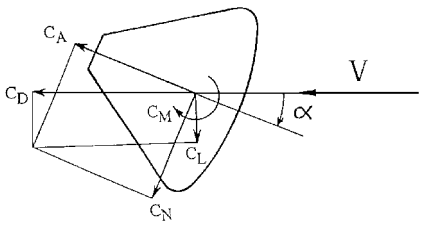

Fig. 3 Model and coordinate axis.

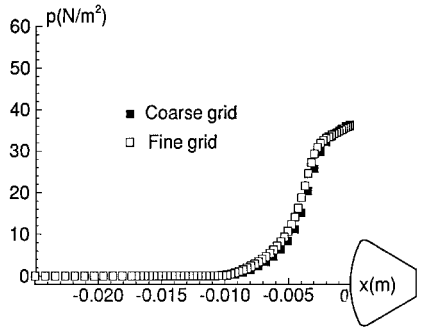

Fig. 4 Pressure distributions; grid sensitivity.

4) the protecting cone is removed from the test section with simultaneous measurements of forces applied to the model after the flow is established, and 5) the cone is once again moved in through the test section to protect the model when shutting down the nozzle flow after test completion. Figure 3 shows the model and coordinate axis.

Numerical Calculations

A zonal finite volume time marching code[8] that solves the complete NS equations has been used to obtain the numerical results. In this code, the evaluation of the inviscid terms is based on a splitting technique in combination with upwind-biased differencing. The code supports the flux-vector-splitting method of Steger and Warming,[9] and the diffusion terms are evaluated using standard central differences. The system of equations is solved using the Gauss–Seidel relaxation algorithm. Viscosity is evaluated using Sutherland's law, and conductivity is obtained by assuming a constant Prandtl number. At these low-density conditions, the code includes velocity slip and temperature jump at the wall using the same boundary conditions formulation as in Ref. 10. The code available was conceived to solve only two-dimensional or axisymmetric configurations. For this reason, only 0-deg angle-of-attack cases were considered. The computational domain was large enough so that upstream and side boundaries were specified as freestream conditions and flow quantities were extrapolated at the downstream boundary. For each test case, numerical results were obtained using both slip and no-slip boundary conditions. The sensitivity of numerical results to mesh refinement was analyzed. The study showed that the cell sizes at the body surface, of the order of mean free path, were small enough to ensure the grid independancy for the numerical aerodynamic coefficients. Thus, the mesh size and number of cells were chosen as a function of the flow rarefaction level. Figure 4 shows the calculated pressure distribution along the symmetry axis (stagnation line) ahead of the model. The results correspond to test conditions referenced as A in Table 1, and were obtained using two levels of mesh refinement. The dark squares correspond to the coarse grid (100 × 40 cells) and the open squares correspond to the fine grid (150 × 70 cells). Near the wall, the cell sizes in both directions (along and perpendicular to wall) were reduced by a factor of two in the fine-grid case. As shown in this figure, the results exhibit a small difference in pressure distributions. The grid refinement causes a change of less than 1% in aerodynamic force coefficients and, finally, all results were carried out using the fine grid.

Experimental and Calculated Data

Force coefficients and moments obtained at the present experimental conditions are compared with previous measurements performed on similar model geometries[3,4] at the Arnold Engineering Development Center (AEDC) and at the Deutsche Luft and Raumfahrt [DLR, German Aerospace Research Establishment (DLR)]. Experimental data are also compared with calculated values using the NS solver.

The drag coefficient of the module is presented in Fig. 5 vs the Reynolds number based on the model diameter and on flow conditions behind a normal shock. At 0-deg angle of attack, drag measurements cover the range between continuum flow and free-molecular flow limits. The drag coefficient results from shear stress and wall-pressure contributions. As shown in Fig. 5, drag values calculated by the NS solver with slip boundary treatment are found to be in good agreement with all experimental results. For lower Reynolds numbers, NS results with no-slip wall boundary conditions are diverging noticeably from the experimental data. At the highest flow rarefactions, the important increase in the calculated drag originates from the shear stress component of the drag. For example, for test conditions A, from NS with wall-slip boundary conditions, the shear stress drag component is about 16% of the total amount of drag, whereas, from NS without wall-slip boundary conditions, the shear stress component represents 27% of the total drag. Furthermore, the continuum approach (e.g., NS) predicts a thiner boundary layer and, consequently, a higher shear stress as compared with a molecular approach (e.g., DSMC).[6] From these results, continuum method with slip boundary treatment predicts drag coefficients accurately for Reynolds numbers as low as $Re_2 = 10$. It appears from the present results that $Re_2 = 10^2$ represents an appropriate limit beyond which a continuum approach (without special boundary treatment) provides reasonable predictions of aerodynamic forces.

Aerodynamic forces applied to re-entry modules have also been measured at various angles of incidence. The angles range from 0 to 50 deg. Investigated experimental test conditions correspond to transitional and near-continuum flow regimes. The axial-force coefficient is plotted in Fig. 6 vs angle of attack. The axial-force coefficient has a maximum value at 0-deg angle of incidence and

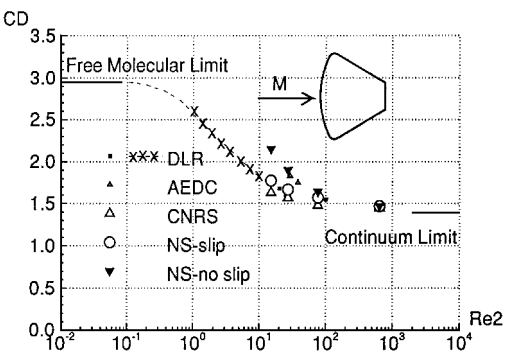

Fig. 5 Drag coefficient at zero angle of attack.

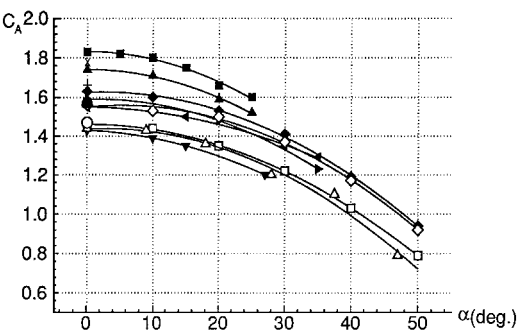

Fig. 6 Axial force coefficient. AEDC results: ■, M = 10.2 and Re_2 = 29; ▲, M = 10.2 and Re_2 = 38; and ▼, M = 11.9 and Re_2 = 55, 200. DLR results: ►, M = 22 and Re_2 = 25 and ◄, M = 12 and Re_2 = 100. CNRS/SR3 results: ♦, M = 20.2 and Re_2 = 15.8; ◊, M = 20.2 and Re_2 = 28.4; □, M = 20.2 and Re_2 = 81; and △, M = 20.9 and Re_2 = 688. NS plus slip boundary conditions results; ○, M = 20.9 and Re_2 = 6.88; ●, M = 20.2 and Re_2 = 81; +, M = 20.2 and Re_2 = 28.4; and ×, M = 20.2 and Re_2 = 15.8.

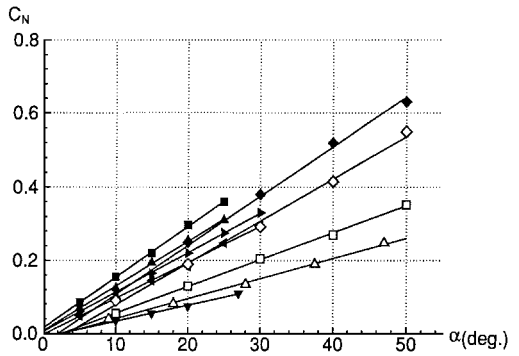

Fig. 7 Normal force coefficient. AEDC results: ■, M = 10.2 and Re_2 = 29; ▲, M = 10.2 and Re_2 = 38; and ▼, M = 11.9 and Re_2 = 55, 2000. DLR results: ►, M = 22 and Re_2 = 25 and ◄, M = 12 and Re_2 = 100. CNRS/SR3 results: ♦, M = 20.2 and Re_2 = 15; ◊, M = 20.2 and Re_2 = 27; □, M = 20.2 and Re_2 = 81; and △, M = 20.9 and Re_2 = 688.

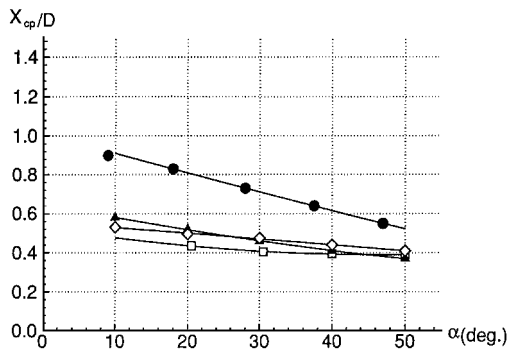

Fig. 8 Center of pressure. CNRS/SR3 results: □, M = 20.2 and Re_2 = 15; ▲, M = 20.2 and Re_2 = 27; ◊, M = 20.2 and Re_2 = 81; and ●, M = 20.9 and Re_2 = 688.

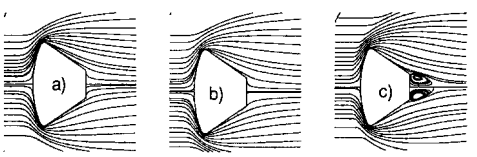

Fig. 9 Streamlines.

corresponds to the drag coefficient. When angle of attack is increased from 0 to 50 deg, the coefficient decreases continuously. For the same angle of incidence and Mach number, the axial-force coefficient increases markedly with higher rarefaction levels within the frame of present test conditions covering continuum and transitional flow regimes. Distributions of the normal-force coefficient are presented in Fig. 7. They show the coefficient to increase when higher angles of incidence and more rarefied flow conditions are considered. As an example, for an angle of incidence of 50 deg and a Mach number close to 20, the normal-force coefficient increases from 0.25 to 0.62 when Re_2 values decrease from 688 to 15.

Besides axial-force and normal-force coefficients, center-of-pressure locations represent useful information to predict the dynamic stability of the module. The balance measurements of the center of pressure along the axis of symmetry of the model are presented in Fig. 8 vs the angle of incidence. The maximum uncertainty on X_{cp}/D is less than 5% for most of the investigated test conditions. The origin of the abscissa is the nose of the module. The center of pressure is found to slightly approach the model nose when higher values of angle of attack are considered. The displacement of the center of pressure is less noticeable for the most rarefied conditions. At the highest flow density, the center of pressure appears to deviate markedly from its location for the other flow rarefactions. This trend could be explained, at the highest density, by the presence of a vortex near the base section of the model. Figure 9 shows flowfield streamlines obtained for test conditions B, C, and D as referenced in Table 1. The model diameter was 45 mm. A vortex appears in the wake region at the highest flow density (Fig. 9).

Conclusion

Investigations have been made to characterize the aerodynamic behavior of re-entry modules at rarefied and hypersonic flow conditions. Experiments have been conducted at a Mach number close to 20 and at rarefied flow conditions covering the near-continuum and transitional flow regimes.

Drag coefficients, axial- and normal-force coefficients, and centers of pressure have been presented as a function of the flow rarefaction and for angles of attack ranging from 0 to 50 deg. Data are compared with previous experimental results and also with NS calculations including both slip and no-slip wall boundary conditions. For the capsule configuration considered, 0-deg angle-of-attack NS computations with wall-slip boundary conditions accurately predicted the drag coefficient in the continuum and transitional flow regimes characterized by a Reynolds number Re_2 larger than 10 (based on the module diameter and the flow conditions behind a normal shock). Without wall-slip boundary conditions, the Reynolds number $Re_2 = 10^2$ appears to represent the lowest limit for estimating aerodynamic forces by a continuum approach.

Acknowledgment

The present research was carried out with the support of the Centre National d'Etudes Spatiales (CNES Evry) under Contract C5-PE-0-1009-LA.

References

[1]Cazaux, C., Watillon, P., and Durand, G., "Atmospheric Reentry Demonstrator: a Flight Experiment for Technology Qualification within the European Manned Space Transportation Programme," *Proceedings of the Second European Symposium on Aerothermodynamics for Space Vehicles*, European Space Agency, Noordwijk, The Netherlands, 1994.

[2]Crowder, R. S., and Moote, J. D., "Apollo Entry Aerodynamics," *Journal of Spacecraft and Rockets*, Vol. 6, No. 3, 1969, pp. 302–307.

[3]Moseley, W. C., Moore, R. H., and Hughes, J. E., "Stability Characteristics of the Apollo Command Module," NASA TN D-3890, March 1967.

[4]Koppenwallner, G., Legge, H., and Muller, H., "Apollo Command Module Aerodynamic Simulation Test in Hypersonic Flow," DLR, German Aerospace Research Establishment, DLR FB Rept. 71-83, Gottingen, Germany, 1971.

[5]Chpoun, A., Lengrand, J. C., Cohen, L., and Heffner, K. S., "Numerical and Experimental Investigation of Rarefied Compression Corner Flow," AIAA Paper 92-2900, July 1992.

[6]Chpoun, A., Cohen L., Lengrand, J. C., Allègre, J., and Raffin M., "Numerical and Experimental Investigation of Rarefied Hypersonic Flow About an ASTV Re-Entry Body," *Proceedings of the Second European Computational Fluid Dynamics Conference*, edited by S. Wagner, E. H. Hirschel, J. Periaux, and R. Piva, Wiley, Chichester, England, UK, 1994. pp. 737–743.

[7]Bird, G.A. "Definition of Mean Free Path for Real Gases," *Physics of Fluids*, Vol. 26, Nov. 1983, pp. 3222, 3223.

[8]Anon., "INCA User's Manuel," Amtec Engineering Inc., Bellevue, WA, May 1993.

[9]Steger, J. L., and Warming, R. F., "Flux Vector Splitting of the Inviscid Gasdynamics Equations with Applications to Finite-Difference Methods," *Journal of Computational Physics*, Vol. 40, 1981, pp. 263–293.

[10]Gupta, R. N., Scott, C. D., and Moss, J. N. "Slip-Boundary Equations for Low-Reynolds-Number Multicomponent Gas Flows," AIAA Paper 84-1732, June 1984.

B. A. Bhutta
Associate Editor